processes

*Article*

# Quantitative Prediction of Deep Coalbed Methane Content in Daning-Jixian Block, Ordos Basin, China

**Zheyuan Ouyang [1,2], Haichao Wang [1,2,*], Bin Sun [3,*], Yunxuan Liu [1,2], Xuehai Fu [4], Wei Dou [1,2], Liang Du [1,2], Beixi Zhang [1,2], Bing Luo [1,2], Mengmeng Yang [1,2] and Zhiwei Zeng [1,2]**

1 Xinjiang Key Laboratory for Geodynamic Processes and Metallogenic Prognosis of Central Asian Orogenic Belt, Xinjiang University, Urumqi 830047, China; ouyang42@stu.xju.edu.cn (Z.O.); xjuliuyunxuan@163.com (Y.L.); douwei0929@163.com (W.D.); duliang0626@163.com (L.D.); zhangbici1231@163.com (B.Z.); lb15890438375@126.com (B.L.); m15827046400@163.com (M.Y.); zengzhiwei0729@163.com (Z.Z.)
2 School of Geological and Mining Engineering, Xinjiang University, Urumqi 830047, China
3 Department of Uncoventionals, Research Institute of Petroleum Exploration and Development, Petrochina, Langfang 065000, China
4 School of Resources & Earth Science, China University of Mining & Technology, Xuzhou 221008, China; fuxuehai@163.com
* Correspondence: wangxiaoshi2111@163.com (H.W.); s-bin@petrochina.com.cn (B.S.)

**Abstract:** The potential of deep coalbed methane resources is substantial. Gas content is an important parameter for resource assessment. At present, the gas content test method commonly used for shallow coal reservoirs is not suitable for determining deep coalbed methane gas content. Therefore, it is urgent to establish a prediction method for deep coalbed methane gas content. This study aims to quantitatively predict the gas content of coalbed methane in deep coal reservoirs and uncover its influencing factors. For this purpose, we selected the Daning-Jixian area, a region in China with relatively advanced development of deep coalbed methane, as a case study. It established a prediction model for adsorbed gas and free gas content in deep coal reservoirs through a series of experimental tests, encompassing gas content, coal quality, isothermal adsorption, and nuclear magnetic resonance. The model sheds light on the impact of coal-rock characteristics, coal quality attributes, and pore characteristics on adsorbed gas and free gas content. The results show that adsorbed gas dominates in deep coal reservoirs with a high metamorphic degree and that the average proportion of adsorbed gas under reservoir burial depth is 80.15%. At a depth of approximately 1800~2000 m, a turning point is observed where adsorbed gas content begins to decline. Beyond this depth range, the detrimental effect of temperature on coalbed methane content surpasses the beneficial impact of pressure. Coal quality characteristics play a major role in controlling adsorbed gas content, and an increase in water content and ash yield significantly reduces the adsorption performance of coal reservoirs. The content of free gas increases with the increase in burial depth, with its controlling factors primarily being confining pressure and porosity. The increase in the proportion of micropores in the pores of deep coal reservoirs has an adverse effect on the content of free gas. The proportion of adsorbed gas in deep coal reservoirs gradually decreases with the increase in burial depth, while the proportion of free gas gradually rises with the increase in burial depth. The development potential of free gas cannot be overlooked in the exploration and development of deep coalbed methane.

**Keywords:** deep coalbed methane; gas content; absorbed gas; free gas; high-rank coal; Daning-Jixian block



**Citation:** Ouyang, Z.; Wang, H.; Sun, B.; Liu, Y.; Fu, X.; Dou, W.; Du, L.; Zhang, B.; Luo, B.; Yang, M.; et al. Quantitative Prediction of Deep Coalbed Methane Content in Daning-Jixian Block, Ordos Basin, China. *Processes* **2023**, *11*, 3093. https://doi.org/10.3390/pr11113093

Academic Editor: Vladimir S. Arutyunov

Received: 6 September 2023
Revised: 19 October 2023
Accepted: 20 October 2023
Published: 27 October 2023



## 1. Introduction

In the United States, Russia, Australia, and India, which have the largest proven coal reserves in the world, the exploration and extraction of coalbed methane has broad prospects [1]. The risk of shallow coal seam mining is relatively high, and the extraction of coalbed methane will effectively avoid this problem [2–4]. According to the new round of exploration results, Chinese deep coalbed methane is more abundant than shallow resources, about $30.37 \times 10^{12}$ m$^3$ [5]. Currently, significant advancements in deep coalbed methane exploration have been accomplished in China, particularly within the Daning-Jixian block of the Ordos Basin and the Baijiahai uplift in the eastern segment of the Junggar Basin. Among these, the production wells of Jishen 6–7 Ping 01 well, DJ17–1 well, JS-01 well, and Caitan 1H well have achieved daily gas production of $10.1 \times 10^4$ m$^3$, $8.0 \times 10^3$ m$^3$, $9.5 \times 10^4$ m$^3$, and $5.7 \times 10^4$ m$^3$, respectively, indicating a promising development prospect [6]. Gas content is a crucial parameter in the computation of deep coalbed methane reserves [7]. It plays a pivotal role in precisely forecasting gas content during the exploration and exploitation of deep coalbed methane resources.

At present, the determination methods of coalbed methane content are mainly divided into direct methods and indirect methods. Previous studies have directly estimated the total gas content based on in situ desorption data. In 1973, the United States Bureau of Mines (USBM) developed the USBM direct method through the methane emission research plan [8]. The gas content encompasses three distinct components: encompassing the natural gas quantity liberated from the borehole into the coal seam before the introduction of the coal sample to the desorption vessel (escaped gas content), the coalbed methane volume released naturally from the coal sample within the desorption tank under standard atmospheric pressure and reservoir temperature conditions (desorption gas content), and the residual coalbed methane quantity within the coal sample subsequent to complete desorption (residual gas content). With the increasing depth of coalbed methane exploration, formation temperature and formation pressure have become the primary influencing factors of gas content testing. The heat preservation and pressure holding coring technology, which maintains the sample at in situ formation temperature, pressure, and shape, has become the main method for testing deep coalbed methane gas content. The current pressure and temperature preservation system (PTPS) is essentially sealed by a ball valve, while the accumulator maintains the pressure, and the temperature is primarily regulated by the active thermal insulation technology of the Japanese oil company PTCS and the passive thermal insulation technology of the gravity piston sampler of Zhejiang University [9,10]. In addition, the gas content in the coal reservoir can be indirectly calculated according to the related properties of coal and its interaction with methane. Wei et al. used the material balance equation to construct the equilibrium kinetic model of coalbed methane generation, migration, accumulation, and loss and quantitatively described a series of processes of coalbed methane occurrence, migration, and loss [11]. Fu et al. used the analytic hierarchy process (AHP), fuzzy mathematics, and the optimal segmentation method to predict gas content based on logging curve parameters [12]. Liu et al. used seismic logging and the multiple linear regression model to predict gas content [13]. Lu et al. used machine learning models and hydrological correction parameters to estimate coalbed methane content [14].

At present, research on the content of deep coalbed methane primarily focuses on qualitatively analyzing its influencing factors. Many factors influence the gas content of coalbed methane, including external geological conditions (temperature and pressure) [15–17] and internal compositional factors (coal-rock characteristics and coal quality characteristics) [18–21]. The differences in these factors result in variations in the content and occurrence of coalbed methane in deep coal reservoirs [16]. Pressure and temperature changes at different burial depths affect the adsorption characteristics of coal and the occurrence state of coalbed methane, consequently influencing the gas content in the reservoir [22–24]. Concurrently, the coal quality characteristics and pore characteristics of coal influence gas content in coal by controlling the storage space of gas in coal reservoirs [25]. Studies have indicated that vitrinite typically develops micropores and exhibits stronger gas adsorption capacity than inertinite [26]. Regarding coal reservoirs spanning different coal ranks, there exists a positive correlation between the level of metamorphism and the coal's capacity for gas adsorption [27]. Broadly, gas content distribution in medium and high-rank coal reservoirs typically comprises roughly 80% to 90% adsorbed gas content, 10% to 20% free gas content, and generally less than 1% dissolved gas content [28–30].

At present, research into deep coalbed methane within the eastern fringes of the Ordos Basin predominantly centers on the examination of variables impacting adsorbed gas quantities [19,31–33]. There are limited studies on predicting free gas content and the variation of adsorbed gas and free gas content with burial depth. Due to the relatively higher proportion of free gas in deep coalbed methane compared to shallow reservoirs, the error in gas loss estimated by the conventional desorption method is significant, leading to a substantial deviation in the final measured gas content.

This study focuses on investigating the gas content of deep coalbed methane within the Daning-Jixian block using a combination of isothermal adsorption, nuclear magnetic resonance, carbon dioxide adsorption, nitrogen adsorption, and high-pressure mercury injection experiments. A predictive model was developed to estimate the quantities of adsorbed and free gas in deep coal reservoirs within the research area. The model's impact on adsorbed and free gas content of deep coalbed methane was elucidated through analyses of coal quality attributes and pore characteristics. The findings of this research hold significant implications for the exploration and development of deep coalbed methane within the studied region.

## 2. Geological Setting

The Ordos Basin is a relatively mature coal-bearing basin in China, covering an area of about $25 \times 10^4$ km$^3$. The basin consists of six secondary tectonic units, namely the Yimeng Uplift, the Western Edge Fault Belt, the Tianhuan Depression, the Yishan Slope, the Jinxi Fault-fold Belt, and the Weibei Uplift [34]. The Daning-Jixian block, where the study area is situated, resides in the southeastern margin of the basin and is a key region for deep coalbed methane development (Figure 1). This study area encompasses a large west-dipping monocline, situated within two tectonic units, including the Guyi-Yaoqu uplift and the Xueguan-Yukou depression [35]. The faults primarily follow a NE or NNE direction [36]. The main coal-bearing strata belong to the Carboniferous–Permian period, comprising the Shanxi Formation and the Taiyuan Formation. On the eastern edge of the Ordos Basin, the development of late Paleozoic coal measures was controlled by differential subsidence in the north–south direction, and the burial depth continued to increase during the Triassic period, with a maximum burial depth of up to 4000 m. From the end of the Indosinian period to the beginning of the Yanshan period, the overall uplift of the structure caused the coal cover to undergo erosion, and the geothermal gradient gradually increased, reaching a maximum of 4.5 °C/100 m in the early Cretaceous period. In the late Yanshan period, the structure was comprehensively uplifted, and the erosion became more intense, resulting in shallower or exposed coal seams. After the Himalayan period, the Cenozoic strata were far from sufficient to compensate for the erosion thickness of the original cover layer of the coal measures [37,38].

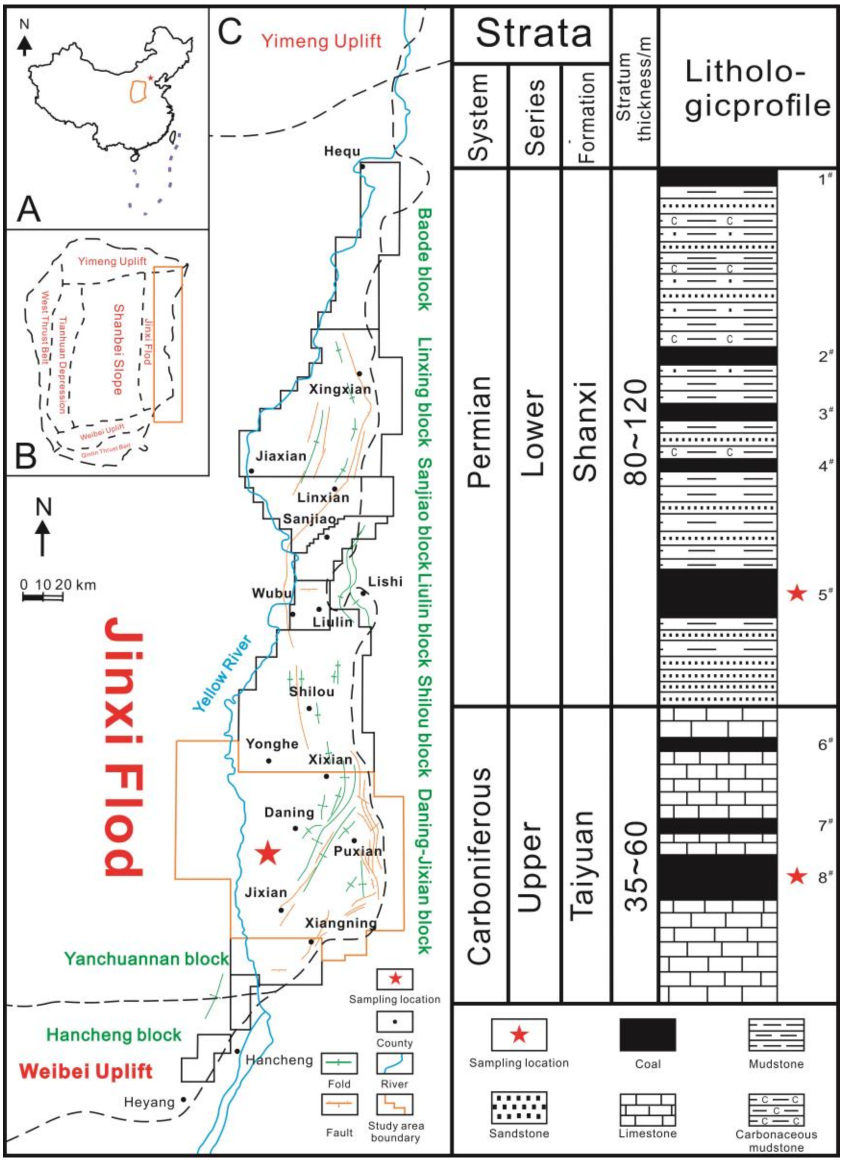


**Figure 1.** Study block location and stratigraphic columnar profile (modified after [20,36]).

## 3. Samples and Methods

### *3.1. Samples Collection and Basic Parameters*

This study involved the collection of 7 coal samples, extracted at depths spanning 2195.30~2277.03 m, from the #5 coal seam of the Shanxi Formation and the #8 coal seam of the Taiyuan Formation, all of which were primary structural coal. The procurement of samples adhered to the guidelines stipulated in the national standard GB/T 212-2008 [39], and subsequent to collection, the samples were promptly transported to the laboratory for rigorous analysis. The maximum vitrinite reflectance ($R_{o,max}$), microscopic composition analysis and coal quality analysis (Table 1) were conducted using the Axio Scope.A1 Zeiss polarizing microscope(Zeiss, Guangzhou, China) and the 5E-MAG6700I industrial analyzer(Kaiyuan Instrument; Changsha, China), respectively. For the sample set, the maximum vitrinite reflectance ranges from 2.93~3.21%, indicating a high metamorphic anthracite composition. The moisture content ranges between 0.70~1.26%, the ash yield ranges from 5.75~15.04%, and the volatile yield ranges between 6.54~10.21%, all of which fall into the ultra-low range.

**Table 1.** Properties of coal samples used in experiments.

| Sample | Depth (m) | $R_{o,m}$ (%) | $\rho_t$ (%) | $\rho_a$ (%) | $\Phi$ (%) | Proximate Analysis (%) | | | |
|---|---|---|---|---|---|---|---|---|---|
| | | | | | | $M_{ad}$ | $A_{ad}$ | $V_{ad}$ | $FC_{ad}$ |
| EP20-1 | 2195.30 | 2.93 | 1.41 | 1.39 | 5.15 | 1.06 | 12.56 | 7.24 | 79.14 |
| EP20-2 | 2196.46 | 3.14 | 1.37 | 1.36 | 5.80 | 0.78 | 5.75 | 6.76 | 86.71 |
| EP20-3 | 2197.00 | 3.30 | 1.43 | 1.38 | 5.41 | 1.00 | 6.76 | 6.54 | 85.70 |
| EP20-4 | 2274.46 | 3.15 | 1.40 | 1.39 | 7.14 | 0.76 | 12.60 | 10.12 | 76.52 |
| EP20-5 | 2275.00 | 3.21 | 1.44 | 1.38 | 6.80 | 0.70 | 15.04 | 7.12 | 77.14 |
| EP20-6 | 2276.40 | 3.21 | 1.40 | 1.35 | 6.67 | 1.26 | 6.41 | 6.56 | 85.77 |
| EP20-7 | 2277.03 | 3.15 | 1.41 | 1.35 | 6.13 | 1.06 | 8.31 | 7.30 | 83.33 |

Note: $R_{o,m}$—maximum reflectance of vitrinite; $\rho_t$—true density; $\rho_a$—apparent density; $\Phi$—porosity; $M_{ad}$—moisture (as received basis); $A_{ad}$—ash (as received basis); $V_{ad}$—volatile (as received basis); and $FC_{ad}$—fixed carbon (as received basis).

### *3.2. NMR Measurement and Isothermal Adsorption Experiment*

The porosity measurement was carried out using the Reccore-04 nuclear magnetic resonance analyzer from Langfang Branch Institute in Research Institute of Petroleum Exploration and Development. The NMR porosity parameters were set to an echo interval (TE) of 0.6 ms, salinity uniform of 33,000 ppm, waiting time (TW) of 5 s, maximum echo count of 2048, and scanning numbers of 64.

All samples were subjected to NMR measurements under two conditions, one being 100% water saturation ($\varphi_w$) and another being dry ($\varphi_d$). The porosity of this article is:

$$\Phi = \varphi_w - \varphi_d, \tag{1}$$

The gravimetric adsorption instrument utilized for this study comprises essential components, including a gas source, booster pump, gas buffer chamber, sample chamber, balance, process control system, and a unit for data acquisition and analysis. The operational parameters of the instrument encompass a maximum experimental pressure threshold of 30 MPa, accurate to within 0.1%, a maximum temperature limit of 110 °C, precise temperature control within 0.5 °C, and temperature readings with a precision of 0.1 °C. The typical sample weight employed is approximately 100 g, and the readings are obtained with a high level of accuracy at 0.001 g. The specific steps are as follows: (1) All coal samples must first be crushed and sieved to 60–80 mesh. (2) Calibrate the balance and observe whether the readings are stable. (3) Tighten the outer casing, fill it with a certain pressure of helium gas (generally 0.5 MPa), and then close the gas valve. After ten minutes, read the pressure value and check for air tightness. (4) Fix the heat-insulating and heat-preservation sleeve around the balance and heating device, connect the temperature sensor and wire, and complete the preparatory work before the experiment. (5) Pressurize the reference cell with $CH_4$ to the predetermined pressure, subsequently unseal the valve connecting the two cells to enable the $CH_4$ transfer from the reference cell to the sample cell. Allow the pressure within the reference cell to steadily decrease over a span of 8–12 h, reaching an equilibrium value that facilitates $CH_4$ adsorption onto the coal matrix surface. Proceed with the adsorption experiment following the temperature, pressure, and duration parameters outlined in the experimental plan. (6) After the experiment is completed, reduce the gas pressure in the sample cell to atmospheric pressure, disassemble the sample cell step by step in the opposite order, remove the sample, and store it properly. The $CH_4$ adsorption measurement of this sample was conducted at a temperature of 333 K. Adsorption data were recorded at nine equilibrium pressures through incremental pressure adsorption, with a maximum value of about 25.5 MPa. The results of the isothermal adsorption experiment are shown in Table 2.

**Table 2.** Isothermal adsorption experimental results.

| Sample | $T_e$ (°C) | $V_L$ ($m^3$/t) | $P_L$ (MPa) |
|---|---|---|---|
| EP20-1 | 60 | 28.795 | 30.401 |
| EP20-2 | 60 | 29.937 | 30.492 |
| EP20-3 | 60 | 31.242 | 29.812 |
| EP20-4 | 60 | 37.097 | 32.126 |
| EP20-5 | 60 | 34.693 | 32.460 |
| EP20-6 | 60 | 35.885 | 29.050 |
| EP20-7 | 60 | 35.589 | 32.179 |

## 4. Prediction of Adsorbed Gas and Free Gas Content

### *4.1. Prediction of Absorbed Gas Content*

The adsorbed gas content in deep coal reservoirs can be represented by the adsorption isotherm in the graphical form of the adsorption state equation. The coal sample employed in this study is a highly metamorphic grade; the isotherm exhibits a Type I isotherm pattern without evident hysteresis, which is a characteristic feature commonly associated with microporous solids. Furthermore, given that the majority of methane adsorption in coal occurs within micropores [40], it becomes imperative to forecast the adsorbed gas content.

The Langmuir monolayer adsorption model, rooted in kinetic theory, stands as the most extensively employed adsorption model. Its basic assumptions are as follows: the adsorption process only forms a monolayer; the solid surface is uniform; the adsorption capacity is the same everywhere; and there is no interaction between the adsorbed molecules [41]. The methane adsorption onto coal is a physical adsorption process taking place on the solid surface and adhering to the Langmuir isotherm adsorption equation. Based on the Langmuir constants obtained from isotherm adsorption experiments, the adsorbed gas content $V_e$ (experimental temperatures) is calculated separately using the Langmuir equation at different pressures, as follows:

$$V_e = \frac{V_L P_e}{P_e + P_L}, \tag{2}$$

where $V_e$ is the amount of gas adsorbed, $m^3/t$; $P_e$ is the equilibrium adsorption pressure, MPa; $V_L$ is the volume of Langmuir, $m^3/t$; and $P_L$ is the Langmuir pressure, MPa. By utilizing Equation (2), the isothermal adsorption experiments yield the amount of gas adsorbed at different temperatures and pressures. Furthermore, considering the impact of reservoir temperature at various burial depths on the adsorbed gas content, the adsorbed gas content $V_r$ (reservoir temperature) is separately calculated at the corresponding reservoir temperature, as follows:

$$V_r = V_e - \Delta V_T \cdot (T_r - T_e), \tag{3}$$

where $V_r$ is the dry ash-free adsorbed gas content at reservoir temperature, $m^3/t$; $T_r$ is the reservoir temperature at different burial depths, °C; $T_e$ is the isothermal adsorption test temperature, °C; and $\Delta V_T$ is the decay rate of methane adsorption for the corresponding coal grade coal sample, $m^3/t \cdot °C$. $\Delta V_T$ reflects the effect of temperature on the methane adsorption in the reservoir under different burial depth conditions. The relationship between methane adsorption in deep coal reservoirs and temperature can be obtained by isothermal adsorption experiments on seven anthracite coal samples. The adsorption capacity of coal decreases with increasing temperature [42]. Through Chen's study [43], it was found that the samples showed some differences in the degree of adsorption variation at different temperatures, with anthracite coal using 45 °C as the cut-off temperature, where pressure below 45 °C controlled the adsorption more than temperature, and vice versa above 45 °C. The Langmuir model calculates that below 45 °C, the adsorption capacity decreases by an average of 0.08577 $m^3/t$ for each 1 °C increase in temperature; above 45 °C the adsorption capacity decreases by an average of 0.10908 $m^3/t$ for each 1 °C increase in temperature, i.e., the decay rate of methane adsorption capacity is 0.08577 $m^3/t\cdot°C$ (<45 °C) and 0.10908 $m^3/t\cdot°C$ (>45 °C). After further analysis of the isothermal adsorption experimental data of coal samples with lower degree of metamorphism in the study area, the decay rates of methane adsorption for long-flame coals and bituminous coals in the study area were found to be 0.02023 $m^3/t\cdot°C$ (<45 °C) and 0.04468 $m^3/t\cdot°C$ (>45 °C). The methane adsorption capacity of coal samples gradually increased by temperature as the degree of deterioration increased. The dry ash-free base sorption gas content at different temperatures and pressures was converted to the sorption gas content at different burial depths of coal reservoirs by the component parameter proximate analysis obtained from the industrial analysis of the samples, as follows:

$$V_A = \frac{V_r \cdot (100 - M_{ad} - A_{ad})}{100}, \tag{4}$$

where $V_A$ is the in situ adsorption gas content at different burial depths, $m^3/t$; $M_{ad}$ is the moisture content, %; and $A_{ad}$ is the ash yield, %. By combining Equations (2)–(4), the total calculation equation of adsorbed gas is obtained as follows:

$$V_A = \frac{[V_L P_e - \Delta V_T \cdot (P_e + P_L)(T_r - T_e)] \cdot (100 - M_{ad} - A_{ad})}{100 \cdot (P_e + P_L)}, \tag{5}$$

*4.2. Prediction of Free Gas Content*

Free gas in coal reservoirs is mainly stored in the pores and micro-fractures of coal seams, and its content is controlled by various geological factors. The main factors include porosity, water saturation, temperature, and pressure conditions. The interplay among these factors contributes to variations in the free gas content within coal reservoirs. When evaluating the potential of free gas in coal reservoirs, a comprehensive analysis of these controlling factors is required. Porosity refers to the ratio of pore volume to the total volume of coal body, which directly affects the gas storage capacity of coal reservoirs. Generally, a higher porosity leads to a higher content of free gas in coal reservoirs [44]. Water saturation quantifies the extent to which pore spaces within coal seams are filled with water. With elevated levels of water saturation, a greater portion of pore space becomes filled with water, leading to a decrease in coalbed methane storage capacity. Temperature and pressure conditions serve as pivotal parameters in the formation and storage mechanisms of coal seam gas. As burial depth increases, the temperature and pressure within coal reservoirs gradually escalate, promoting the generation and storage of coal seam gas.

At present, the calculation of the free gas content in unconventional oil and gas reservoirs is mostly based on gas state equations and Marriotte's law, combined with relevant national standards (SY/T 6040-2013) [45] and (NB/T 10018-2015) [46]. This study relies on the unconventional natural gas free gas content model to estimate the free gas content within deep coal reservoirs [47]:

$$V_F = \frac{\Phi S_g}{\rho_a B_g}, \tag{6}$$

where $V_F$ is the free gas content of the reservoir, $cm^3/g$; $\Phi$ is the porosity, %; $S_g$ is the gas content saturation, %; $\rho_a$ is the apparent density of coal, $g/cm^3$; and $B_g$ is the methane gas volume factor, dimensionless. The methane gas volume coefficient $B_g$ is calculated as follows:

$$B_g = \frac{V_g}{V_{sc}}, \tag{7}$$

where $V_g$ is the volume of nmol gas under ground conditions, $cm^3$ and $V_{sc}$ is the volume of nmol gas in the ground standard state, $cm^3$; this is combined with the true gas state equation Equation (7) as follows:

$$PV = nRTZ, \tag{8}$$

where P is pressure, MPa; T is temperature, K; Z is gas compression factor; n is the amount of gas substance, mol; and R is the gas constant. The expression of the methane gas system number is obtained as:

$$B_g = \frac{P_{sc}ZT}{PT_{sc}}, \quad (9)$$

where $P_{sc}$ is pressure under standard state, MPa and $T_{sc}$ is temperature under standard state, K.

Combining Equations (5)–(8), the prediction equation for the free gas content of deep coalbed methane is obtained as:

$$V_F = \frac{\Phi S_g P T_{sc}}{\rho_a P_{sc} Z T}, \quad (10)$$

## 5. Result and Discussion

### *5.1. Adsorbed Gas in Deep Coal Reservoir*

#### 5.1.1. Adsorbed Gas Content under Reservoir Conditions

According to Equation (5), the adsorption gas content of coal at varying burial depths can be calculated by substituting ash and moisture data derived from Langmuir parameters and coal quality tests (Figure 2). The adsorbed gas content ranges from 18.12~28.34 $m^3/t$, showing an initial increase followed by a decline as the coal seam burial depth increases. This phenomenon arises due to the heightened stress and temperature sensitivity of deep coal reservoirs in comparison to their shallower counterparts. In conjunction with Equation (5), it is evident that formation temperature and pressure exert opposing influences on the adsorption and gas content of deep coal reservoirs. When other formation conditions remain unaltered, an elevation in formation pressure augments coal's gas adsorption capacity, resulting in a positive pressure effect. Conversely, heightened formation temperature enhances the thermal activity of coalbed methane, consequently weakening the coal's gas adsorption capacity, manifesting as a negative temperature effect. Under certain burial depth conditions, the positive and negative effects achieve equilibrium, leading to an inflection point between adsorbed gas content and the burial depth of the coal reservoir [22].

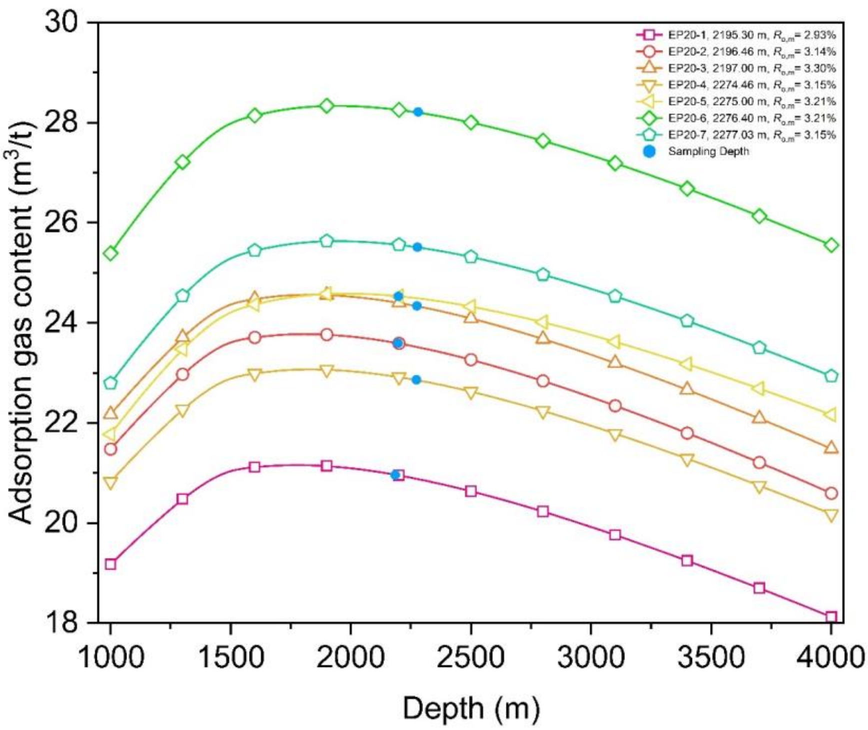


**Figure 2.** Prediction of adsorbed gas content at different buried depths.

The adsorbed gas content within the sample experienced rapid growth below 1600 m. For instance, considering the EP20-5 sample, the adsorbed gas content surged from 21.74~24.37 $m^3/t$, constituting a rise of 12.10%, primarily driven by the positive pressure effect. Between 1600~2000 m, the adsorbed gas content displayed a relatively stable trend, with an increase from 24.37~24.59 $m^3/t$, representing a minor increment of 0.90%. At this juncture, the positive pressure effect and the negative temperature effect on adsorbed gas exerted approximately equal influence. When the burial depth surpasses 2000 m, the adsorbed gas content gradually declined with the escalating burial depth, decreasing from 24.59~22.16 $m^3/t$ at 4000 m, marking a reduction of 9.88%. In this phase, it is commonly accepted that the negative temperature effect outweighs the positive pressure effect, resulting in a progressive reduction in adsorbed gas quantity as burial depth and reservoir temperature increase.

As we know, coalbed methane predominantly exists in an adsorbed state within coal reservoirs, constituting over 90% of the total gas content in coal seams [48]. In shallower regions, the gas content of coalbed methane rises with increasing burial depth. To be more specific, high metamorphic coal within the shallower portion, at burial depths less than 1000 m, exhibits an upward trend in gas content as burial depth increases. In contrast, the adsorbed gas content of highly metamorphic coal in this study manifests a pattern of initial growth followed by decline within the burial depth range of 1000~4000 m. The point at which this trend in adsorbed gas content shifts is approximately within the range of 1800~2000 m (Figure 2), and it exhibits a more conspicuous positive correlation with reflectivity (Figure 3).

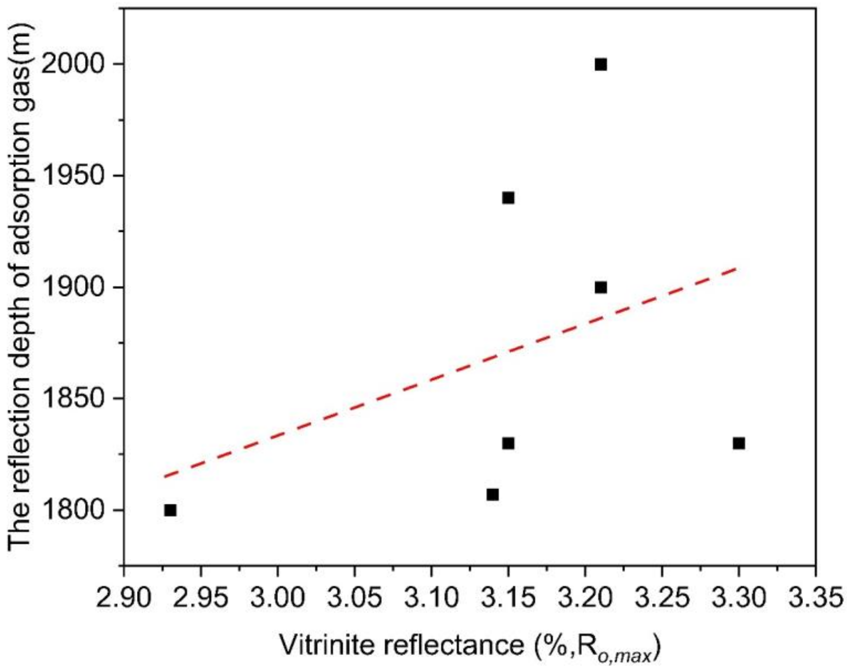


**Figure 3.** Relationship between the reflection depth of adsorption gas and vitrinite reflectance.

### 5.1.2. The Influence of Coal-Rock Characteristics and Coal Quality Characteristics on Adsorbed Gas

It is widely accepted that the primary factors influencing the adsorption characteristics of deep coalbed methane are categorized as external geological conditions and internal material composition. External geological conditions primarily involve temperature and pressure, while internal material composition primarily encompasses coal-rock characteristics, including microscopic coal-rock components, as well as coal quality characteristics such as ash and water content.

The coal petrographic analysis reveals that the samples are primarily high-metamorphic anthracite, with exinite components having decomposed and disappeared. The predominant macerals are vitrinite (41.8~64.3%, averaging at 56.13%) and inertinite (26.6~52.5%, averaging at 36.0%). Vitrinite is the most significant maceral, formed from the gelification of plant roots, stems, and leaves under overlying water's reducing conditions. The adsorbed gas content exhibits a positive correlation with the vitrinite content. As the vitrinite content increases, so does the adsorbed gas content in the coal seam (Figure 4). This phenomenon is primarily due to the volatile nature of the vitrinite group at the high metamorphic stage, resulting in more developed micropores. In contrast to the inertinite group, the vitrinite group possesses a larger porous volume and specific surface area, resulting in an augmentation of methane adsorption sites, this enhances the coal seam's adsorption capacity. On the contrary, the inertinite content in the sample exhibits a negative overall correlation with adsorption gas content. This phenomenon can be attributed to the decrease in micropore volume and specific surface area as the inertinite content increases across samples with varying degrees of metamorphism [27]. According to the volume filling theory of methane, adsorbed gas predominantly occupies the micropores. Therefore, under equivalent conditions, high-rank coal samples with a greater vitrinite content exhibit greater adsorption capacity and adsorption space than coal samples with a higher inertinite content.

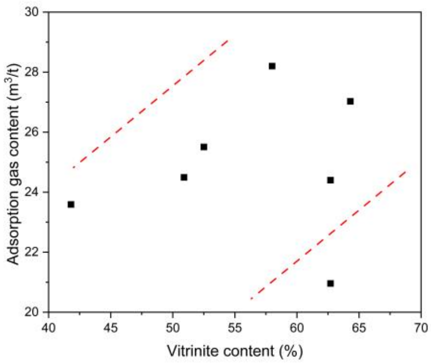


(**a**)

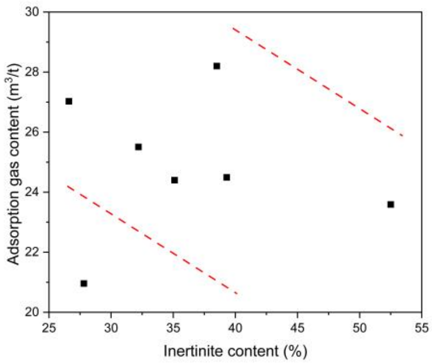


(**b**)

**Figure 4.** Effect of different coal petrographic characteristics on adsorbed gas. (**a**) vitrinite and (**b**) inertinite.

Within the realm of coalbed methane, the primary factors influencing gas adsorption capacity are the moisture and ash content of coal. Moisture in coal pertains to the water either adsorbed or condensed within the pores of coal particles. Because coal has a stronger force on polar bond bound water than van der Waals force bound methane, it will lead to the competition of adsorption sites between water and methane in coal seam [49]; in addition, water molecules can also be combined by dipole motion, which weakens the adsorption capacity of coal gas. Therefore, as the water content in coal samples steadily rises, there is a gradual decrease in the content of adsorbed gas within the coal.

The ash content reflects the content of minerals in coal. The ash content (Ad) of deep samples in the study area is between 5.75~15.04%. The primary constituent of ash in coal is clay minerals, which exhibit weak gas adsorption characteristics. The presence of ash within coal occupies the voids that would otherwise be filled by organic matter. Due to its limited gas−surface affinity, ash diminishes the specific surface area available for organic matter to adsorb gas, occupies gas storage space, and consequently results in a reduction in coal's methane adsorption capacity. Hence, there exists a negative correlation between coal seam ash content and adsorbed gas content, as illustrated in Figure 5.

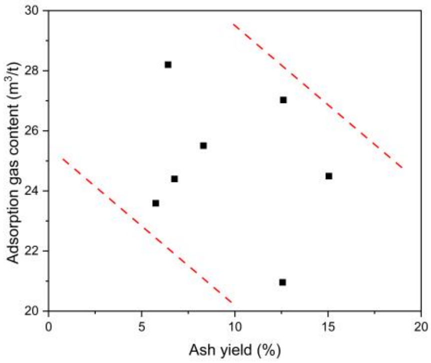


(**a**) (**b**)

**Figure 5.** Effect of different coal characteristics on adsorbed gas. (**a**) ash yield and (**b**) moisture content.

*5.2. Free Gas in Deep Coal Reservoir*

5.2.1. Free Gas Content under Reservoir Conditions

By utilizing the isothermal adsorption parameters and the measured gas content of the coal seam, we can calculate the gas saturation (Sg):

$$S_g = \frac{V_{am}}{V_L} \tag{11}$$

where $V_{am}$ is the measured gas content, $m^3/t$. Then, the reservoir temperature and pressure parameters are substituted into Equation (10) and the free gas content of each sample at the buried depth of 1000~4000 m can be obtained, as illustrated in Figure 6. The findings indicate that the free gas content increases as the burial depth of the coal seam rises. In the case of the same sample, the rate of free gas content increase is gradual with the deepening of burial depth (Figure 6), and the free gas content ranges between 1.54~11.20 $m^3/t$. Combined with the Equation (10), it can be seen that porosity is an important factor affecting the content of free gas when the buried depth of each sample collection horizon is not much different, that is, when the temperature and pressure are similar.

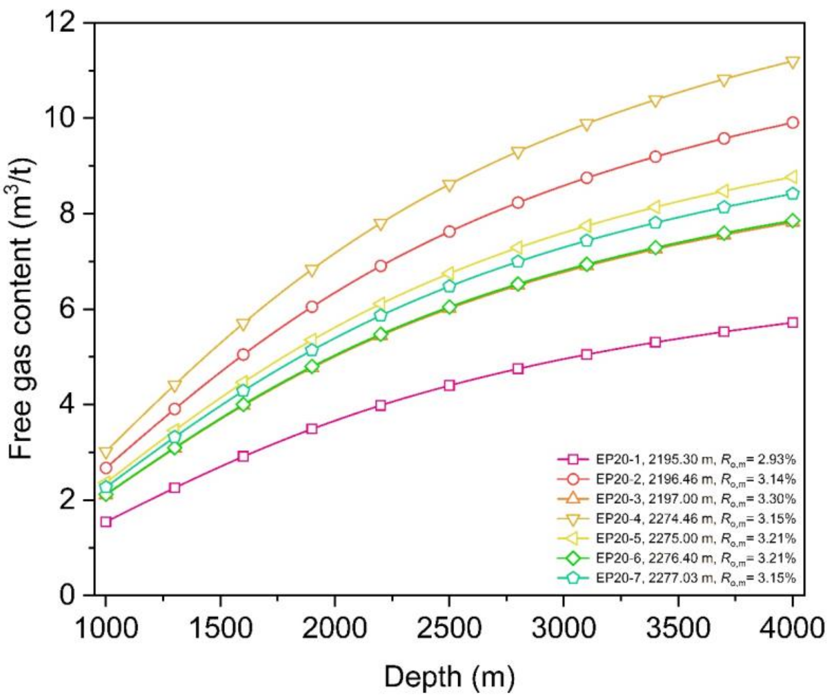


**Figure 6.** Prediction of free gas content at different buried depths.

5.2.2. The Influence of Pore Characteristics on Free Gas

As evident from Equation (10), porosity exhibits a close relationship with free gas content, thereby serving as a pivotal influencing factor. An escalation in porosity signifies an augmentation in gas storage capacity. In the study area, coal porosity ranges from 5.18% to 7.14% and increases in tandem with the elevation of coal rank. This phenomenon starkly contrasts with the observation that porosity in shallow coal reservoirs does not notably change with increased coal rank (Figure 7).

In the current study, the proportion of free gas in low metamorphic coal seams is relatively high. For example, the proportion of free gas in low rank coal in Junggar Basin accounts for a considerable proportion, which is closely related to the pore type dominated by medium and large pores [50]. On the contrary, the coal reservoir in the study area consists of anthracite with a higher degree of metamorphism, where a significant abundance of micropores is prevalent within the coal's vitrinite component, effectively occupying the majority of the pore space [51,52], the pore type is dominated by micropores [53], resulting in enhanced adsorption capacity of pores for gas, CBM is mainly adsorbed, and free gas content is less. This observation also elucidates the positive correlation between the depth at which adsorbed gas undergoes a transition and coal rank within the study area. In other words, as the degree of metamorphism increases, the porosity primarily comprised of micropores expands.

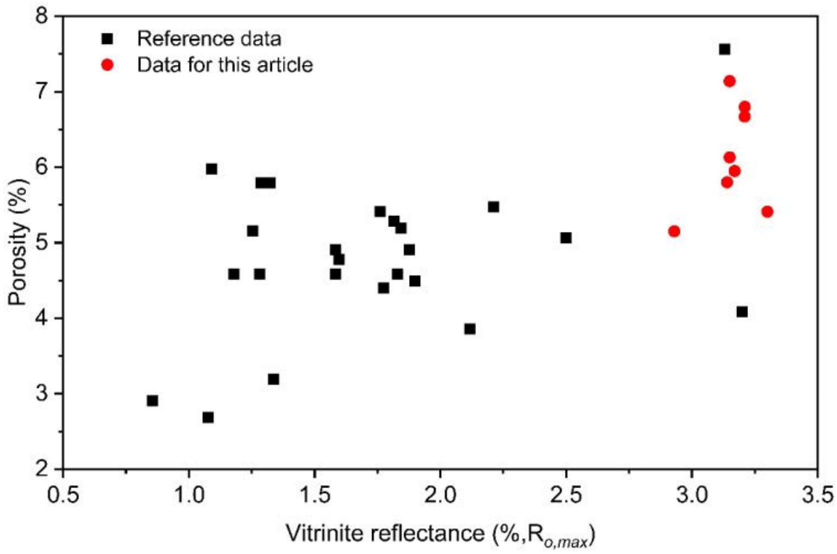


**Figure 7.** Porosity of coals varying with vitrinite reflectance (the data come from [54]).

The specific surface area distribution and pore size distribution of the study area samples were assessed through carbon dioxide adsorption, nitrogen adsorption, and high-pressure mercury intrusion experiments, as depicted in Figures 8 and 9. The BET SSA for the seven samples spanned from 214.40 to 294.40 $m^2/g$, with micropores (<2 nm) accounting for a range of 209.41 to 291.81 $m^2/g$, constituting approximately 98.4% of the total specific surface area. In terms of pore size distribution, micropores, on average, comprised 93.7% of the total pore volume. It shows that in deep coal reservoirs, the porosity of coal is mainly micropores, and micropores contain most of the pore space in the sample, providing a large number of adsorption points for the adsorption of methane by the sample [55]. In contrast to the shallow coal samples exhibiting medium to low metamorphic degrees, the deep coal samples, despite having relatively high porosity, display extensive micropore development, which enhances their adsorption capacity for methane. Consequently, this phenomenon results in a sustained low level of free gas content within the coal seam. This explains why the porosity of coal seams in the deep part of the study area is high but the free gas content is still at a relatively low level, even if its proportion is still higher than that in shallow reservoirs.

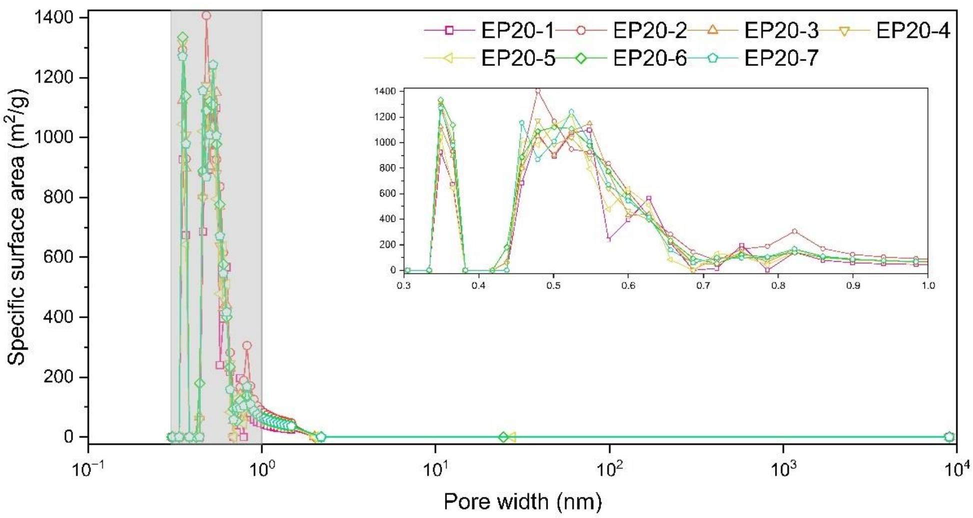


**Figure 8.** The specific surface area of samples.

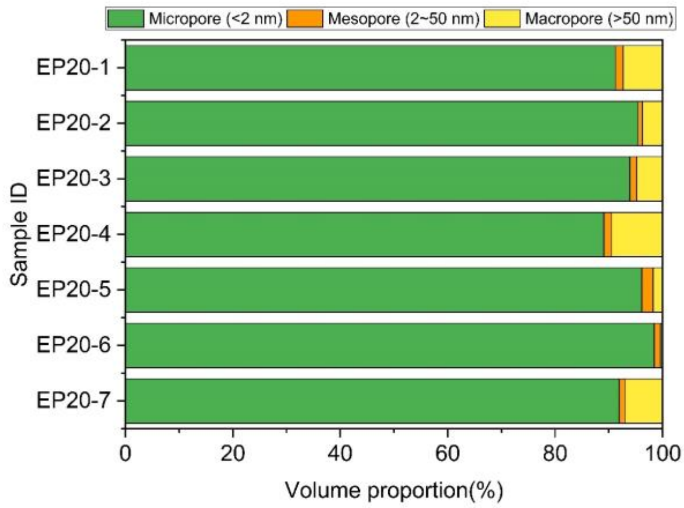


**Figure 9.** The pore size ratio of samples (the macroporous proportion of EP20-6 sample was 0.4%).

*5.3. Total Gas Content of Deep Coal Reservoir*

Following the prediction of adsorbed gas content ($V_A$, $m^3/t$) and free gas content ($V_F$, $m^3/t$) through simulation, the in situ gas content ($V_I$) can be expressed as $V_I = V_A + V_F$. The calculation of in situ gas content is conducted employing the general formula derived from Equations (5) and (10):

$$V_I = \frac{[V_L P_e - \Delta V_T \cdot (P_e + P_L)(T_r - T_e)] \cdot (T_r(100 - M_{ad} - A_{ad})}{100 \cdot (P_e + P_L)} + \frac{\Phi S_g P_r T_{sc}}{\rho_a P_{sc} Z(T_r + 273.15)} \tag{12}$$

where $P_e$ is the equilibrium adsorption pressure, MPa; $V_L$ is the volume of Langmuir, $m^3/t$; $P_L$ is the Langmuir pressure, MPa; $P_r$ is the reservoir pressure at different burial depths, MPa; $T_r$ is the reservoir temperature at different burial depths, °C; $T_e$ is the isothermal adsorption test temperature, °C; $\Delta V_T$ is the decay rate of methane adsorption for the corresponding coal grade coal sample, $m^3/t \cdot °C$; $M_{ad}$ is the moisture content, %; $A_{ad}$ is the ash yield, %.$\Phi$ is the porosity, %; $S_g$ is the gas content saturation, %; $\rho_a$ is the apparent density of coal, $g/cm^3$; $P_{sc}$ is pressure under standard state, MPa; $T_{sc}$ is temperature under standard state, K; and Z is gas compression factor.

By applying Equation (12) and incorporating the regional geological parameters specific to the study area, it becomes possible to perform a comprehensive assessment of the in situ gas content within the deep coal reservoirs in the study area, as detailed in Table 3. The findings indicate that all coal samples within the study area are undersaturated, with an average gas saturation of 71.00%. The measured gas content of EP20-4 coal sample is the highest, which is 29.89 $m^3/t$, and the predicted gas content is 30.87 $m^3/t$. The highest predicted gas content is EP20-6 sample, which is 33.83 $m^3/t$.

**Table 3.** Gas content data of coal samples used in the experiment.

| Sample | Depth (m) | Gas Content ($m^3$/t) | Predict Gas Content ($m^3$/t) | Gas Saturation (%) |
|---|---|---|---|---|
| EP20-1 | 2195.30 | 16.43 | 24.94 | 57.06 |
| EP20-2 | 2196.46 | 26.28 | 30.49 | 87.78 |
| EP20-3 | 2197.00 | 23.20 | 29.84 | 74.26 |
| EP20-4 | 2274.46 | 29.89 | 30.87 | 80.57 |
| EP20-5 | 2275.00 | 22.99 | 30.78 | 66.27 |
| EP20-6 | 2276.40 | 21.72 | 33.83 | 60.53 |
| EP20-7 | 2277.03 | 25.11 | 31.54 | 70.56 |

As illustrated in Figure 10, within the burial depth range of 1000~4000 m, the total gas content of coal reservoirs escalates with increasing depth. However, around the 2500 m mark, a decline in adsorbed gas content within the deep coal reservoir becomes apparent, leading to a deceleration in the rate of total gas content increase. A notable inflection point emerges at approximately 3000 m. Figure 11 reveals a substantial positive correlation between the transition depth of total gas content and the transition depth of adsorbed gas content. This implies that, despite varying burial depths, adsorbed gas continues to exert a dominant influence on the total gas content. The average proportion is 80.15% at the reservoir depth, and the proportion is still 76.05% at the burial depth of 3000 m. At the same time, it should be emphasized that although the proportion of free gas under different burial depths is less than that of adsorbed gas, the proportion of free gas increases with the increase of burial depth. For example, the average proportion of free gas under reservoir depth is 19.85%, and with the increase of burial depth, the average proportion of free gas at the depth of 3000 m increases to 23.95%, with an increase of 20.65% (Figure 12), indicating that compared with shallow coal reservoirs, the free gas content of deep coal reservoirs is considerable, which will lead to deep coalbed methane mining. The characteristics of fast gas discovery, high initial gas production and fast attenuation are different from those of shallow coalbed methane mining.

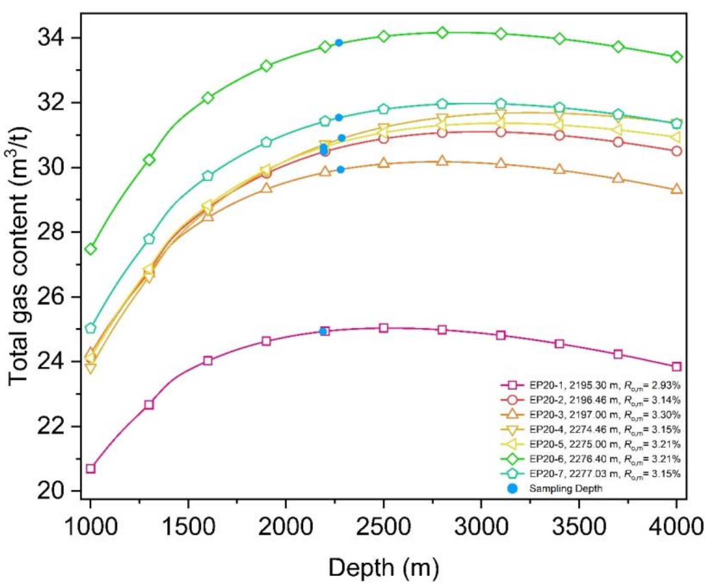


**Figure 10.** Prediction of coalbed methane content in different buried depths.

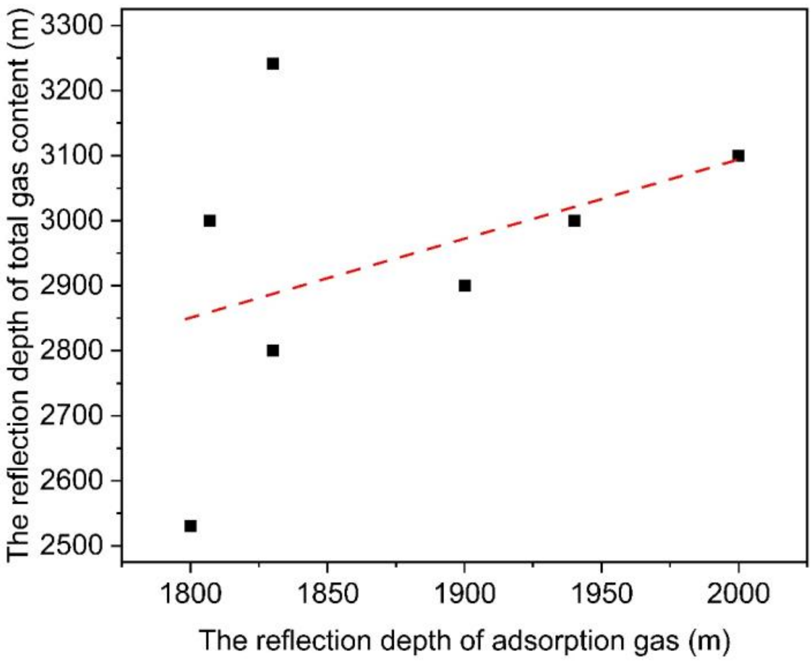


**Figure 11.** The ratio of adsorbed gas to free gas at different buried depths.

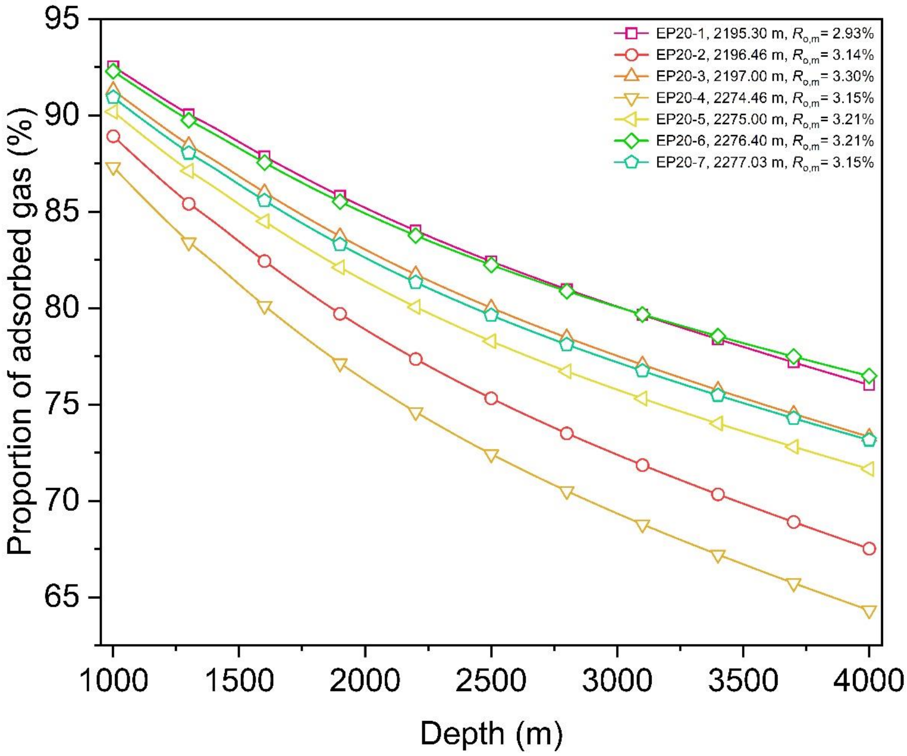


**Figure 12.** The proportion of adsorbed gas under different buried depths.

Due to the large burial depth of deep coal seams, the lifting time in the core recovery process is long and mud blockage occurs easily. In this process, a large amount of gas loss is can occur. This portion of the lost gas primarily comprises free gas, resulting in the final measured gas content being lower than the actual gas content of the reservoir.

In this study, the gas content of seven borehole coal samples collected from deep coal reservoirs in Daning-Jixian was determined by the US Bureau of Mines USBM method [56] and was compared with the predicted value of the total gas content of coal samples obtained by the mathematical model (Figure 13).

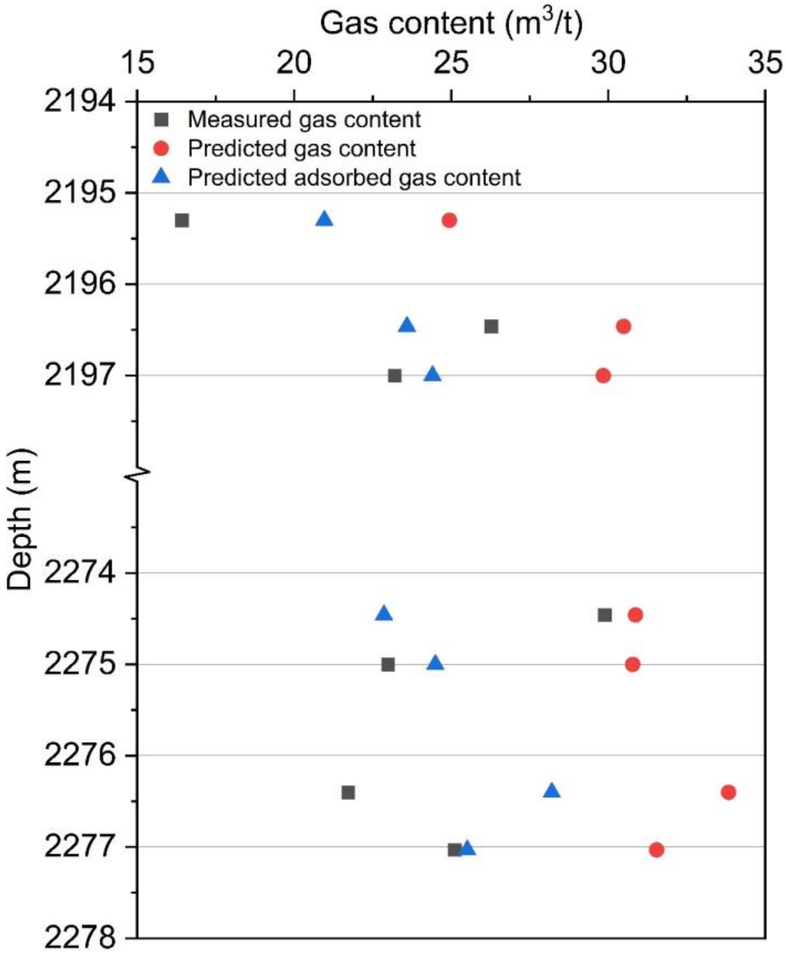


**Figure 13.** Measured gas content, predicted gas content, and predicted adsorbed gas content under different buried depths.

It is important to emphasize that the average ratio of measured total gas content to predicted total gas content stands at 77.88%. Meanwhile, the average ratio of measured total gas content to predicted adsorbed gas content is 97.85%, aligning with the assumption that the lost gas primarily comprises free gas with a minor fraction of adsorbed gas. This observation underscores the relative scientific accuracy of gas content prediction. In future work, we will try other different methods for gas prediction, such as neural networks [57].

## 6. Conclusions

In this study, we investigate the gas content of deep coal reservoirs in the Daning-Jixian area and establish a prediction model for adsorbed gas and free gas content in these reservoirs by integrating experimental testing and mathematical modeling. We predict the adsorbed gas and free gas content of deep coalbed methane in the Daning-Jixian block. Our primary conclusions are outlined as follows:

1. In the depth range of 1000~4000 m, the positive effect of pressure led to an increase in the adsorbed gas content before 1600 m; the negative effect of temperature leads to a decrease in the adsorbed gas content after a burial depth of 2000 m. Through the analysis of coal rock and coal quality, the adsorbed gas content rises with an increase in vitrinite content and diminishes with increased inertinite content, moisture content, and ash yield;

2. In the depth range of 1000~4000 m, there is a gradual increase in free gas content, albeit with a diminishing rate of growth. Under the same temperature and pressure conditions, porosity emerges as the primary factor influencing free gas content. Although higher porosity allows for increased storage of free gas, the existence of numerous micropores within the vitrinite component might, to some extent, diminish the free gas proportion;
3. In the burial depth range of 1000~4000 m, the total gas content of coal reservoir increases first and then decreases with the increase of burial depth. This turning point corresponds to the shift in adsorbed gas content and occurs at an average depth of approximately 3000 m. In this study, adsorbed gas predominates under reservoir conditions, constituting 74.03% to 84.05%, with an average of 80.15%. In contrast, free gas content ranges from 15.95% to 25.97%, averaging 19.85%. Compared with shallow coal seams, the higher free gas content of deep coal seam methane has an impact on resource development that cannot be ignored. This study provides a certain reference for predicting the gas content of deep coal seams in various regions of the world.

**Author Contributions:** Conceptualization, Z.O., H.W. and B.S.; methodology, Z.O. and H.W.; validation, Z.O. and Y.L.; formal analysis, Z.O. and B.L.; investigation, Z.O. and H.W.; resources, B.S. and X.F.; data curation, W.D. and L.D.; writing—original draft preparation, Z.O.; writing—review and editing, H.W., Z.Z., B.Z. and M.Y.; supervision, H.W. and X.F.; project administration, H.W.; and funding acquisition, H.W., B.S. and X.F. All authors have read and agreed to the published version of the manuscript.

**Funding:** This work was funded by the National Natural Science Foundation of China Regional Fund (42262021, 42072190, 41902171); the Xinjiang Uygur Autonomous Region Natural Science Foundation (2022D01C38).

**Conflicts of Interest:** The authors declare no conflict of interest.

## References

1. Ahmed, A.J.; Johnston, S.; Boyer, C.; Lambert, S.W.; Bustos, O.A.; Pashin, J.C.; Wray, A. Coalbed methane: Clean energy for the world. *Oilfield Rev.* **2009**, *21*, 4–13.
2. Bosikov, I.I.; Martyushev, N.V.; Klyuev, R.V.; Savchenko, I.A.; Kukartsev, V.V.; Kukartsev, V.A.; Tynchenko, Y.A. Modeling and Complex Analysis of the Topology Parameters of Ventilation Networks When Ensuring Fire Safety While Developing Coal and Gas Deposits. *Fire* **2023**, *6*, 95. [CrossRef]
3. Liu, Y.; Chang, L.; Zhou, F.; Tan, D.; Liu, L.; Kang, J.; Tian, H. Numerical modeling of gas flow in deformed well casing for the prediction of local resistance coefficients pertinent to longwall mining and its engineering evaluation. *Environ. Earth Sci.* **2017**, *76*, 686. [CrossRef]
4. Malozyomov, B.V.; Golik, V.I.; Brigida, V.; Kukartsev, V.V.; Tynchenko, Y.A.; Boyko, A.A.; Tynchenko, S.V. Substantiation of Drilling Parameters for Undermined Drainage Boreholes for Increasing Methane Production from Unconventional Coal-Gas Collectors. *Energies* **2023**, *16*, 4276. [CrossRef]
5. Geng, M.; Chen, H. Methods and results of the fourth round national CBM resources evaluation. *Coal. Sci. Technol.* **2018**, *46*, 64–68.
6. Li, S.; Wang, C. Reservoir forming characteristics and favorable area evaluation of deep coalbed methane in Daning-Jixian Block. *Coal. Geol. Explor.* **2022**, *50*, 59–67.
7. Li, Y.; Wang, Z. Re-evaluating adsorbed and free methane content in coal and its ad- and desorption processes analysis. *Chem. Eng. J.* **2022**, *428*, 131946. [CrossRef]
8. Kissell, F.N.; McCulloch, C.M. *The Direct Method of Determining Methane Content of Coalbeds for Ventilation Design*; (in press). US Department of Interior, Bureau of Mines: Washington, DC, USA, 1973; Volume 7767.
9. Kawasaki, M.; Umezu, S. Pressure temperature core sampler (PTCS). *J. Jpn. Assoc. Pet. Technol.* **2006**, *71*, 139–147. [CrossRef]
10. Zhu, H.; Chen, J. Status of Cooling Technology for Submarine Natural Gas Hydrate Sampler. *Explor. Eng.* **2017**, *44*, 59–65.
11. Wei, C.; Qin, Y. Simulation study on evolution of coalbed methane reservoir in Qinshui Basin, China. *Int. J. Coal Geol.* **2007**, *72*, 53–69. [CrossRef]
12. Fu, H.; Tang, D. Geological characteristics and cbm exploration potential evaluation: A case study in the middle of the southern Junggar Basin, NW China. *J. Nat. Gas Sci. Eng.* **2016**, *30*, 557–570. [CrossRef]
13. Liu, B.; Chang, S. Coalbed methane gas content and its geological controls: Research based on seismic-geological integrated method. *J. Nat. Gas Sci. Eng.* **2022**, *101*, 104510. [CrossRef]

14. Lu, C.; Zhang, S. Improved estimation of coalbed methane content using the revised estimate of depth and catboost algorithm: A case study from southern Sichuan Basin, China. *Comput. Geosci.* **2022**, *158*, 104973. [CrossRef]
15. Gensterblum, Y.; Merkel, A. Gas saturation and co2 enhancement potential of coalbed methane reservoirs as a function of depth. *Aapg Bull.* **2014**, *98*, 395–420. [CrossRef]
16. Wei, Q.; Li, X. Reservoir characteristics and coalbed methane resource evaluation of deep-buried coals: A case study of the no.13-1 coal seam from the Panji Deep Area in Huainan Coalfield, Southern North China. *J. Petrol. Sci. Eng.* **2019**, *179*, 867–884. [CrossRef]
17. Kang, J.; Fu, X. Vertical heterogeneity of permeability and gas content of ultra-high-thickness coalbed methane reservoirs in the southern margin of the Junggar basin and its influence on gas production. *J. Nat. Gas Sci. Eng.* **2020**, *81*, 103455. [CrossRef]
18. Chatterjee, R.; Paul, S. Classification of coal seams for coal bed methane exploitation in central part of Jharia coalfield, India—A statistical approach. *Fuel* **2013**, *111*, 20–29. [CrossRef]
19. Li, Y.; Cao, D. Variation in maceral composition and gas content with vitrinite reflectance in bituminous coal of the eastern Ordos Basin, China. *J. Petrol. Sci. Eng.* **2017**, *149*, 114–125. [CrossRef]
20. Li, S.; Tang, D. Geological conditions of deep coalbed methane in the eastern margin of the Ordos Basin, China: Implications for coalbed methane development. *J. Nat. Gas Sci. Eng.* **2018**, *53*, 394–402. [CrossRef]
21. Wang, Z.; Fu, X.; Pan, J.; Deng, Z. Effect of $N_2$/$CO_2$ injection and alternate injection on volume swelling/shrinkage strain of coal. *Energy* **2023**, *275*, 127377. [CrossRef]
22. Qin, Y.; Shen, J. On the fundamental issues of deep coalbed methane geology. *Acta. Petrol. Sin.* **2016**, *37*, 125–136.
23. Li, S.; Tang, D. Progress in geological researches on the deep coalbed methane reservoirs. *Earth Sci. Front.* **2016**, *23*, 10–16.
24. Faiz, M.; Saghafi, A. The influence of petrological properties and burial history on coal seam methane reservoir characterisation, Sydney Basin, Australia. *Int. J. Coal Geol.* **2007**, *70*, 193–208. [CrossRef]
25. Liu, L.; Jin, C. Coalbed methane adsorption capacity related to maceral compositions. *Energy Explor. Exploit.* **2020**, *38*, 79–91. [CrossRef]
26. Das, P.R.; Mendhe, V.A. Petrographic and geochemical controls on methane genesis, pore fractal attributes, and sorption of lower Gondwana coal of Jharia Basin, India. *ACS Omega* **2022**, *7*, 299–324. [CrossRef] [PubMed]
27. Jia, T.; Zhang, S. Pore structure and adsorption characteristics of maceral groups: Insights from centrifugal flotation experiment of coals. *ACS Omega* **2023**, *8*, 12079–12097. [CrossRef]
28. Li, X.; Shi, J. Transport mechanism of desorbed gas in coalbed methane reservoirs. *Pet. Explor. Dev.* **2012**, *39*, 203–213. [CrossRef]
29. Gray, I. Reservoir engineering in coal seams: Part 1—The physical process of gas storage and movement in coal seams. *Soc. Pet. Eng.* **1987**, *2*, 28–34. [CrossRef]
30. Gray, I. Reservoir engineering in coal seams: Part 2—Observations of gas movement in coal seams. *Soc. Pet. Eng.* **1987**, *2*, 35–40. [CrossRef]
31. Li, Y.; Yang, J. Unconventional natural gas accumulations in stacked deposits: A discussion of upper paleozoic coal-bearing strata in the east margin of the Ordos Basin, China. *Acta Geol. Sin.* **2019**, *93*, 111–129. [CrossRef]
32. Shen, J.; Li, K. The geochemical characteristics, origin, migration and accumulation modes of deep coal-measure gas in the west of Linxing block at the eastern margin of Ordos Basin. *J. Nat. Gas Sci. Eng.* **2021**, *91*, 103965. [CrossRef]
33. Sun, B.; Shao, Y. Coalbed methane enrichment characteristics and exploration target selection in the zhuozishan coalfield of the western Ordos Basin, China. *ACS Omega* **2022**, *7*, 43531–43547. [CrossRef] [PubMed]
34. Cai, Y.; Liu, D. Preliminary evaluation of gas content of the no. *2 coal seam in the Yanchuannan area, southeast Ordos Basin, China. J. Petrol. Sci. Eng.* **2014**, *122*, 675–689. [CrossRef]
35. Li, C.; Jiang, B. Characteristics of tectonic deformation in the Daning-Jixian region, eastern Ordos Basin: Implications for the exploration and development of coalbed methane. *Energy Explor. Exploit.* **2019**, *37*, 907–921. [CrossRef]
36. Yan, T.; He, S. Critical tectonic events and their geological controls on deep buried coalbed methane accumulation in Daning-Jixian Block, eastern Ordos Basin. *Front. Earth Sci.* **2023**, *17*, 197–217. [CrossRef]
37. Chen, Y.; Tang, D.; Xu, H.; Li, Y.; Meng, Y. Structural controls on coalbed methane accumulation and high production models in the eastern margin of Ordos Basin, China. *Nat. Gas. Geo.* **2015**, *23*, 524–537. [CrossRef]
38. Ren, Z.; Yu, Q.; Cui, J.; Qi, K.; Chen, Z.; Cao, Z.; Yang, P. Thermal history and its controls on oil and gas of the Ordos Basin. *Earth Sci. Front.* **2017**, *24*, 137–148.
39. *GB/T 212-2008*; Proximate Analysis of Coal. Standard Press Of China: Beijing, China, 2008.
40. Clarkson, C.R.; Marc Bustin, R. Variation in micropore capacity and size distribution with composition in bituminous coal of the western Canadian sedimentary basin: Implications for coalbed methane potential. *Fuel* **1996**, *75*, 1483–1498. [CrossRef]
41. Saunders, J.T.; Yang, R.T. Adsorption of gases on coals and heat-treated coals at elevated temperature and pressure. *Fuel* **1985**, *64*, 616–620. [CrossRef]
42. Shen, J.; Qin, Y. Properties of deep coalbed methane reservoir-forming conditions and critical depth discussion. *Nat. Gas. Geo.* **2014**, *25*, 1470–1476.
43. Chen, G.; Li, W. Influencing factors and laws of adsorption capacity of deep coalbed methane in Ordos Basin. *Nat. Gas. Ind.* **2011**, *31*, 47–49.
44. Rodrigues, C.F.; Lemos De Sousa, M.J. The measurement of coal porosity with different gases. *Int. J. Coal Geol.* **2002**, *48*, 245–251. [CrossRef]
45. *SY/T 6040-2013*; Measurement Method of Shale Gas Content. Petroleum Industry Press: Beijing, China, 2014.

46. *NB/T 10018-2015*; Method of Determining Low-Rank Coal Gas Content. China Electric Power Press: Beijing, China, 2016.
47. Lewis, R.; Ingraham, D. New Evaluation Techniques for Gas Shale Reservoirs. In Proceedings of the Reservoir Symposium, Tulsa, OK, USA, 13–17 April 2002.
48. Qin, Y.; Shen, J. Accumulation effects and coupling relationship of deep coalbed methane. *Acta. Petrol. Sin.* **2012**, *33*, 48–54.
49. Pan, Z.; Connell, L.D. Effects of matrix moisture on gas diffusion and flow in coal. *Fuel* **2010**, *89*, 3207–3217. [CrossRef]
50. Yang, M.; Sun, B. *CBM Enrichment Model and Exploration Direction of Baijiahai Uplift in Junggar Basin*; Geology Press: Nanjing, China, 2019; pp. 291–297.
51. Harris, L.A.; Yust, C.S. Transmission electron microscope observations of porosity in coal. *Fuel* **1976**, *55*, 233–236. [CrossRef]
52. Zhang, S.; Tang, S. The characteristics of coal reservoir pores and coal facies in Liulin district, Hedong coal field of China. *Int. J. Coal Geol.* **2010**, *81*, 117–127. [CrossRef]
53. Nie, B.; Liu, X. Pore structure characterization of different rank coals using gas adsorption and scanning electron microscopy. *Fuel* **2015**, *158*, 908–917. [CrossRef]
54. Zhang, K.; Tang, D. Study on influence factors of adsorption capacity of different metamorphic degree coals. *Coal. Sci. Technol.* **2017**, *45*, 192–197.
55. Du, X.; Cheng, Y. $CO_2$ and $CH_4$ adsorption on different rank coals: A thermodynamics study of surface potential, Gibbs free energy change and entropy loss. *Fuel* **2021**, *283*, 118886. [CrossRef]
56. Diamond, W.P.; Schatzel, S.J. Measuring the gas content of coal: A review. *Int. J. Coal Geol.* **1998**, *35*, 311–331. [CrossRef]
57. Klyuev, R.V.; Morgoev, I.D.; Morgoeva, A.D.; Gavrina, O.A.; Martyushev, N.V.; Efremenkov, E.A.; Mengxu, Q. Methods of Forecasting Electric Energy Consumption: A Literature Review. *Energies* **2022**, *15*, 8919. [CrossRef]